Article

Plasmonic Nano Silver: An Efficient Colorimetric Sensor for the Selective Detection of Hg^{2+} Ions in Real Samples

Nasir Mahmood Abbasi [1], Muhammad Usman Hameed [2], Najma Nasim [3], Farid Ahmed [4,*], Faizah Altaf [3], Shabnam Shahida [2], Sana Fayyaz [3], Syed Mubashar Sabir [2] and Patrizia Bocchetta [5,*]

1   College of Engineering and Applied Sciences, Nanjing University, Nanjing 210093, China; abbasichemist786@gmail.com
2   Department of Chemistry, University of Poonch, Rawalakot 12350, Pakistan; drusmanhamid@upr.edu.pk (M.U.H.); shabnamshahida01@gmail.com (S.S.); syedmubasshar@upr.edu.pk (S.M.S.)
3   Department of Chemistry, Women University of Azad Jammu & Kashmir, Bagh 12500, Pakistan; najmanasim12@gmail.com (N.N.); faizahaltaf@gmail.com (F.A.); sanafayyaz777@gmail.com (S.F.)
4   Institute for Advanced Study Shenzhen University, Shenzhen 518060, China
5   Department of Innovation Engineering, University of Salento, Edificio La Stecca, Via per Monteroni, 73100 Lecce, Italy
*   Correspondence: farids_ahmed@yahoo.com (F.A.); patrizia.bocchetta@unisalento.it (P.B.)

Abstract: Environmental pollution caused by heavy metal ions has become a major health problem across the world. In this study, a selective colorimetric sensor based on starch functionalized silver nanoparticles (St-Ag NPs) for rapid detection of Hg^{2+} in real samples was developed. The environmentally friendly green approach was utilized to synthesize starch functionalized silver nanoparticles (St-AgNPs). A multi-technique approach involving UV-Vis absorption spectroscopy, Fourier transform infrared (FT-IR), X-ray diffraction (XRD), and scanning electron microscope (SEM) was used for the characterization of St-Ag NPs. These starch functionalized AgNPs were tested for the detection of heavy metals at 25 °C. The screening process revealed clear changes in the AgNPs color and absorption intensity only in the presence of Hg^{2+} due to the redox reaction between Ag^0 and Hg^{2+}. The color and absorption intensity of nanoparticles remain unchanged in the presence of all the other tested metals ion. The proposed method has strong selectivity and sensitivity to Hg^{2+} ions, with a detection limit of 1 ppm revealed by UV-visible spectrophotometry. The proposed procedure was found to be successful for the detection of Hg^{2+} in real samples of tap water.

Keywords: green synthesis; nanotechnology; silver nanoparticles; surface plasmon resonance; calorimetric detection; tap water

1. Introduction

During the last decade, the emerging field of plasmonic-based nanotechnology brought a revolutionary track in the discipline of applied sciences due to many practical applications of nanoparticles in the field of environmental sciences, such as wastewater treatment [1,2]. Heavy metal ions (M$^+$), such as Cr^{3+}, Zn^{2+}, Ni^{2+}, Cu^{2+}, and Hg^{2+}, are essentially mandatory for the growth process of both animals and plants at appropriate concentrations. However, these metal ions are harmful to living creatures at relatively high concentrations because of their input in both human and animal bodies via biological food webs [3,4].

Mercury ion (Hg^{2+}), which is widely distributed in the atmosphere, soil on the earth's surface, and even in water, is one of the most lethal and hazardous metal pollutants [5,6]. There are various sources of mercury such as the burning of coal in power plants, natural liberation of gases from earth surface during vulcanization, and metals extraction process [7]. Hg^{2+} is a persistent pollutant because naturally, it cannot decompose in the environment [8]. In water, fishes consume mercury as it is dissolved in water, and through

the food web, this is the major way of mercury accumulation in humans [9]. It can damage the brain, the nervous system, and the immune system [6].

Therefore, detection of poisonous metals in the aquatic environment and biological system has become a crucial need of the present-day world [10]. During the last decade, various methods have been developed for Hg^{2+} detection, including electrochemical methods [11], optical detections [12], atomic absorption spectroscopy, inductively coupled plasma mass spectroscopy [13], and fluorescent spectroscopy [14]. However, most of these approaches are inconvenient because the use of complicated instruments is painstaking and time-consuming [15,16]. Therefore, the introduction of a logical technique that is not just easy and cheap but also useful and reproducible, and able to sense the toxic metal pollutants in the ecological samples, is greatly needed. For these mentioned problems, approaches to low cost and rapid detection of mercury using silver nanoparticles (AgNPs) or gold nanoparticles (AuNPs) are advantageous [17,18].

Synthesizing metallic nanoparticles (AgNPs and AuNPs) in an environmentally friendly manner is a key step in nanotechnology. In the field of selective and sensitive detection methods, the use of environmentally friendly nanotechnology has recently become increasingly significant [19,20]. During the last decade, colorimetric sensors, in particular, have a distinct advantage because of their versatility, rapidity, high selectivity, and ease of use, which includes the ability to perform real-time qualitative [19] and quantitative analysis [21,22].

Nanotechnology has the potential to boost life sciences, healthcare, and industrial technology significantly. For example, Lax man et al. [23] presented an optical process for careful recognition of Hg^{2+} depending upon the aggregation of AgNPs. Wang et al. [24] reported a highly sensitive method for sensing Hg^{2+}, ascorbic acid, and Cd^{2+} by using trithiocy anuric acid gold NPs. Senapati and co-workers, in their work, showed the use of tryptophan coated gold nanoparticles for selective and efficient detection of Hg^{2+} [25]. Chai et al. [26] presented colorimetric detection of Pb^{2+} using glutathione functionalized AuNPs. However, these approaches typically use some chemicals as reducing agents that frequently produce toxic side products [27]. Some of them used organic reagents as the functional selective reagents, which are unstable and easily oxidized, while some tagging agents found it costly to use these techniques as sensors for real life [28]. Additionally, the production processes of nanoparticles used in sensing systems are complex [29]. These sensors are generally derivatives of fluorescent dyes, usually harmful to the environment [30,31].

Colorimetric detection of particular analytes of interest by using AuNPs and AgNPs is a common practice because of color changes which are simply viewed with naked eyes instead of complicated instruments [32]. These nanoparticles are used as colorimetric probes for sensing lethal metal ions from ecological samples via cheap and simple procedures [33]. Compared to AuNPs, silver nanoparticles have several benefits such as low cost, easy preparation, etc. Further, AgNPs can also be oxidized by Hg^{2+}, which causes color change and decrease in the UV-visible UV spectrum absorption of the AgNPs.

Besides the other advantages, the role of surfactant during the synthesis of AgNPs is very important. The starch and D-glucose are biomolecules that are non-toxic and biocompatible ligands. Starch acts as a protecting agent as it contains many hydroxyl (–OH) groups that will simply attach to the surface of AgNPs through the Ag-O bond and prevent the accumulation of AgNPs [34]. The use of silver nitrate was reduced by D-glucose in the presence of starch synthesizes nanoparticles (NPs). D-Glucose is an ecologically favorable and mild reducing agent, which is activated in the presence of a basic catalyst.

In this paper, a fast and very selective colorimetric method was developed for the detection of Hg^{2+} by using starch-functionalized AgNPs, with a green synthesis approach. The addition of Hg^{2+} to AgNPs solution produces instant color change (dark yellow to colorless) which can be seen by the naked eye. The selectivity of this detection system of Hg^{2+} by using starch stabilized AgNPs is outstanding when compared with other metal ions such as Pb^{2+}, Al^{3+}, Zn^{2+}, Cu^{2+}, and Fe^{3+}. Additionally, the detection process of

Hg^{2+} is outstanding even in the presence of a mixture of the mentioned heavy metal ions. Furthermore, AgNPs were successfully employed for the detection of Hg^{2+} ion in real water samples.

2. Materials and Methods

2.1. Chemicals

$AgNO_3$, KOH, KCl, NaCl, $FeCl_3$, $ZnCl_2$, $HgCl_2$, $NiCl_2 \cdot 6H_2O$, $CuSO_4$, and $AlCl_3$ were purchased from Sigma Aldrich. D-glucose and soluble starch $((C_6H_{10}O_5)_n)$ were also purchased from Sigma Aldrich. Distilled water was used during the research. All the required substances were received in pure form so there was no need for additional purification.

2.2. Synthesis of Starch-Stabilized AgNPs

In a typical synthetic procedure, 2 mL of D-glucose (0.1 M), 2 mL of starch (0.2 wt%), and 0.02 mL of KOH (0.1 M) were added into 5 mL of $AgNO_3$ (10 mM). After that, the mixture was heated at 30 °C for 10 min with continuous stirring at (100 rpm). After that formation of AgNPs was indicated by a color change from colorless to deep reddish yellow. The basic steps involved during the synthesis process are mentioned in Scheme 1. This nanoparticle dispersion was centrifuged at 1200 rpm to obtain solid particles. Finally, the prepared nanoparticles were stored at 25 °C for further characterization.
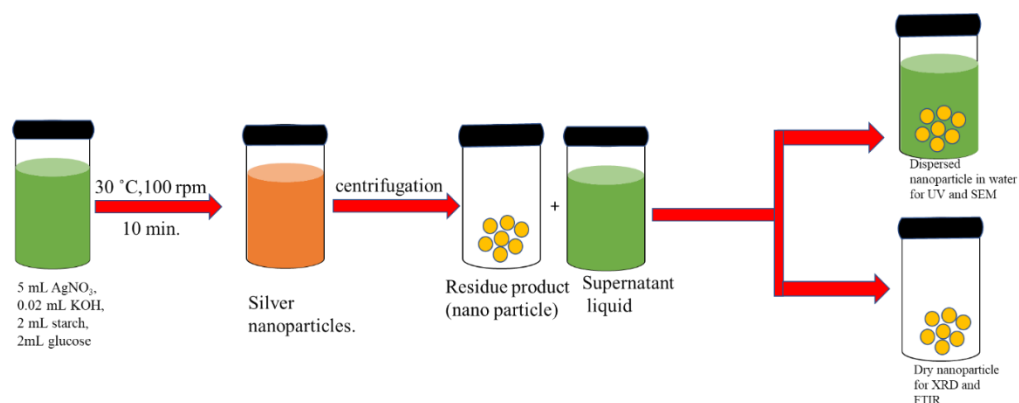
Scheme 1. Different steps involved in the preparation of AgNPs.

2.3. Characterization

The synthesized AgNPs were analyzed first by UV-vis spectrophotometer. UV-vis absorption studies were done by using UV-1800 double beam spectrophotometer (Shimadzu, Kyoto, Japan), utilizing quartz cuvettes of 1.0 cm path length in the UV range from 200–800 nm. XRD was recorded on a Bruker D-8 powder X-ray diffractometer by Cu-K radiation ($\lambda = 0.15418$ nm) over a range of 20–90° with a step size of 0.02°. FT-IR spectra were obtained by using FT-IR 8400S Shimadzu, Japan using KBr disk (4000–400 cm^{-1}).

2.4. General Procedure for the Calorimetric Determination of Hg^{2+}

For detection of Hg^{2+} using AgNPs dispersion, 1 mL (100 ppm) of aqueous solutions of Pb^{2+}, Cu^{2+}, Al^{3+}, Zn^{2+}, Fe^{2+}, Ni^{2+}, and Hg^{2+} were added, respectively, into 1 mL of AgNPs dispersion. To find out the detection limit, various concentrations of $HgCl_2$ (1–100 ppm) were prepared from the stock solution by quantitative dilution. Keeping the total volume of mixture constant (2 mL), an equal volume of Ag-NPs and $HgCl_2$ (each concentration) were mixed. To check out the selectivity of the detection system 100 ppm aqueous solutions of Pb^{2+}, Cu^{2+}, Al^{3+}, Zn^{2+}, Fe^{2+}, Ni^{2+}, and Hg^{2+} were prepared. 1 mL of every solution was added into 1 mL solution of Hg^{2+} (100 ppm) and 1 mL of AgNPs dispersion. All the solution and dilution processes were carried out at room temperature.

To determine the binding stoichiometry of Hg^{2+} and AgNPs, Hg^{2+} (100 ppm) solution ratios from 0.1 to 2 mL were mixed with AgNPs dispersion in opposite ratios of volume. To find out the role of pH on the sensing study, pH of AgNPs was varied from 1 to 12. To study the practical applications of the planned strategy, we used tap water for Hg^{2+} detection. About 100 ppm Hg^{2+} solution was prepared in tap water, and then 1 mL of that dispersion was mixed with AgNPs dispersion in tap water. All of these mixtures were kept at room temperature for 10 min to monitor the effect of Hg^{2+} on AgNPs dispersion in tap water.

3. Results and Discussions

3.1. Visual Detection of AgNPs Synthesis

The color of the reaction mixture changed within 10 min from colorless to reddish yellow (as shown in Figure 1A), after mixing starch, glucose, and KOH solution with $AgNO_3$ solution. Thus, Ag^+ reduction was confirmed as the colorless silver nitrate solution altered to yellowish-brown. It is assumed that the production of AgNPs is a redox reaction where Ag^+ is reduced to Ag^0 with the oxidation of glucose to corresponding gluconic acid which was later on confirmed through FT-IR.
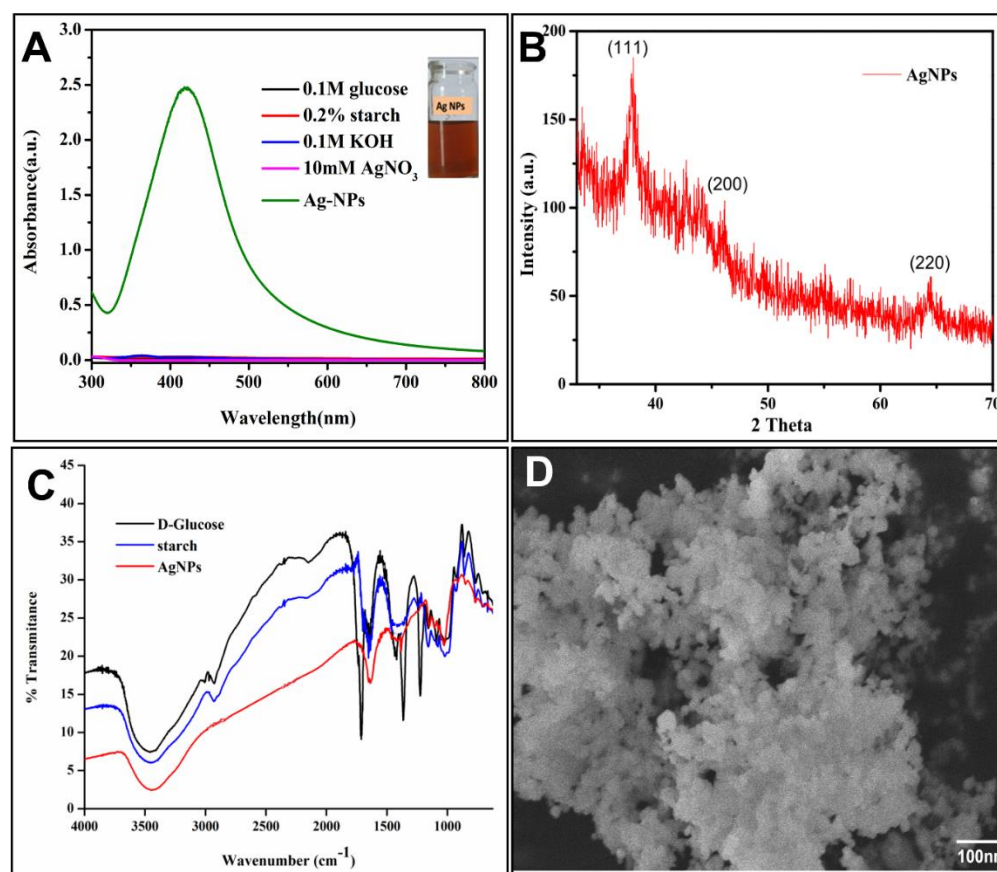

Figure 1. (**A**) UV spectra show Glucose, Starch, KOH, and $AgNO_3$ and synthesized AgNPs, (**B**) XRD image of synthesized silver nanoparticles. (**C**) FT-IR Spectrum of AgNPs and (**D**) SEM image of synthesized AgNPs.

3.2. UV–Visible Absorption Spectroscopy

The synthesized AgNPs were analyzed by UV–visible absorption spectroscopy technique because of the surface plasmon resonance (SPR) phenomenon. When light waves interact with free electrons present in the reduced AgNPs surface, plasmon resonance originates. For confirmation of the formation of AgNPs, UV spectra were recorded for a starch solution, D-Glucose solution, and KOH solution, which do not show any characteristic absorption due to the absence of SPR. UV–vis spectrum of the AgNPs suspensions shows an

absorption maximum at 430 nm, as shown in Figure 1A. As a function of synthesis/reaction time, the absorbance was found to increase and a maximum was observed after a reaction time of 10 min (as depicted in Figure 1, green curve). Thus, the optimum reaction time for the synthesis of AgNPs was found to be 10 min. Under the influence of high temperature, the rate of reduction of Ag^+ increases, and therefore the rapid synthesis of AgNPs could be achieved [35].

3.3. X-ray Diffraction

A characteristic XRD pattern of synthesized AgNPs showed various reflections, at 38.2° (111), 44.3° (200), and 64.5° (220) as shown in Figure 1B. These sharp Bragg peaks maybe produced due to the stabilization of nanoparticles by starch that acts as a capping agent. The peak related to the (111) plane was more prominent than the rest of the planes, signifying that the (111) plane was the major orientation in the face-centered cubic (fcc) structure of AgNPs. The XRD results of AgNPs show a crystalline behavior similar to previously reported literature [36].

3.4. FT-IR Analysis

FT-IR spectra were used to recognize the functional groups in different types of compounds. For comparison, IR spectra were recorded for D-Glucose, starch, and AgNPs. In spectra of D-glucose and starch, there is a wide peak at 3200–3500 cm^{-1}, which reflects the stretching vibration of OH group (i.e., hydrogen-bonded), and a sharp peak at 1725 cm^{-1} represents the C=O stretch of aldehyde group. The sharp peaks at 2900 cm^{-1} and 1100 cm^{-1} are the stretching vibrations of aldehyde C-H and C-O, respectively. Moreover, OH bending vibration is reflected in the region of 1433 cm^{-1}. In IR spectra of AgNPs, the peaks of OH group stretching and bending are less intense. A sharp peak in the region of 1710 cm^{-1} appeared, which indicates the presence of the COOH group as shown in Figure 1C. It means that during the formation of AgNPs, the C=O and OH groups of Starch and D-Glucose cause the reduction of Ag^+ ions from $AgNO_3$ and itself oxidized into respective acid. KumariJyoti et al. reported similar observations in their work [37].

3.5. Scanning Electron Microscopy

The surface morphology monitored by SEM images reveals various shapes in the form of spherical AgNPs. Figure 1D shows the low and high magnification images of AgNPs. One can observe that the particle size lies in the range of 1–100 nm. This may be due to the availability of the different quantities of capping agents during their synthesis process [38].

3.6. Parametric Study of the Synthesis of AgNPs

The volume of $AgNO_3$ (10 mM) (NN-A1 to NN-A5), starch (0.2%) (NN-A6 to NN-A10), and glucose (0.1 M) (NNA-11 to NNA-15) varied from 1 to 5 mL as shown in Table 1. UV spectra showed that absorption gradually increases with theAgNO$_3$ volume ratio. This finding can be associated with the rise in the redox reaction rate involving $AgNO_3$ and the OH groups of starch and glucose, whereas absorption gradually decreases with an increase in the volume ratio of starch and glucose (as shown in Figure 2A–C) due to a simple dilution effect.

Table 1. Experimental details for different volume ratios of $AgNO_3$, starch, and glucose during the synthesis of Ag-NPs.

Sample No.	AgNO$_3$ (mL)	Starch (mL)	Glucose (mL)	KOH (mL)	Temperature (°C)	Stirring (rpm)	Time (min)
NN-A1	1	5	2	0.02	30	100	10
NN-A2	2	5	2	0.02	30	100	10
NN-A3	3	5	2	0.02	30	100	10
NN-A4	4	5	2	0.02	30	100	10

Table 1. *Cont.*

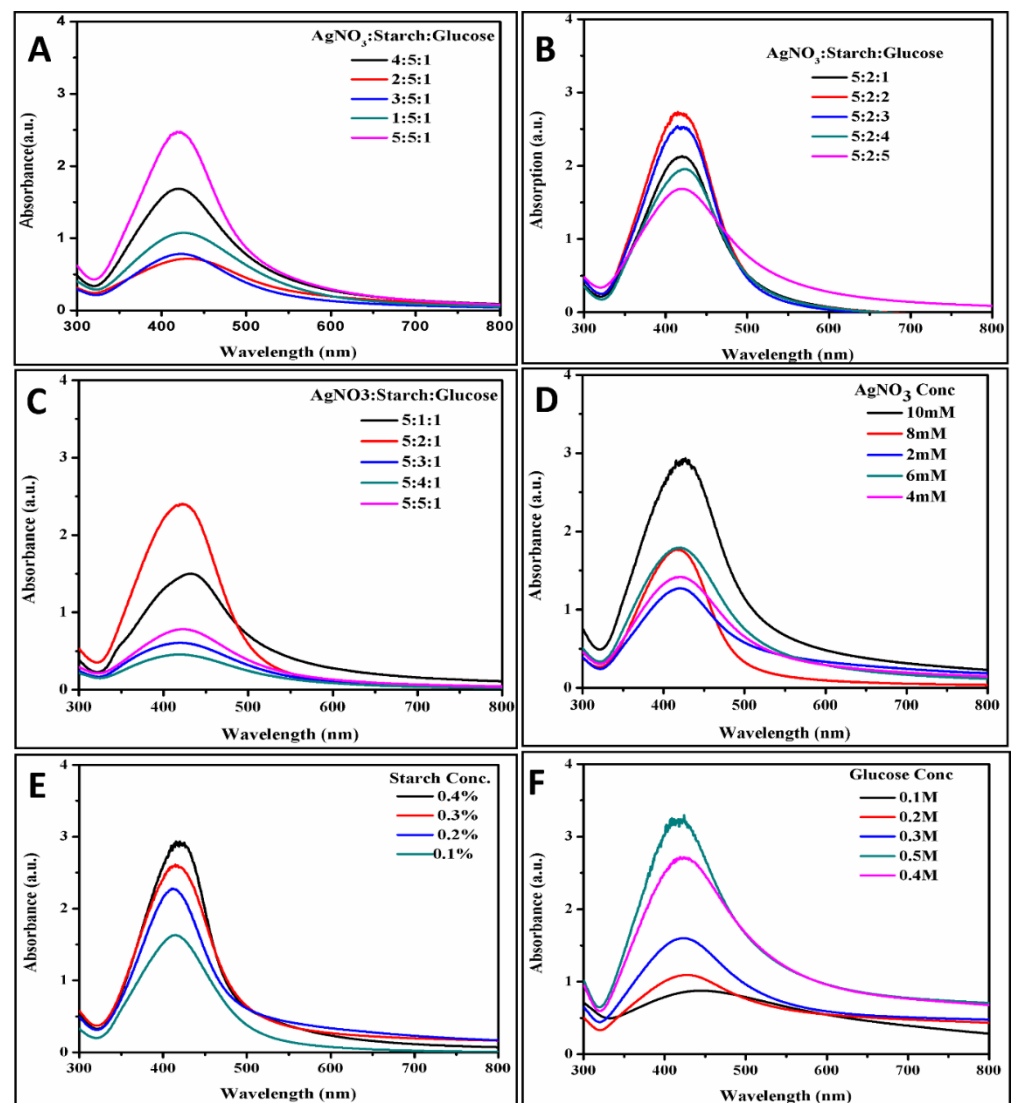| Sample No.	AgNO₃ (mL)	Starch (mL)	Glucose (mL)	KOH (mL)	Temperature (°C)	Stirring (rpm)	Time (min)
NN-A5	5	5	2	0.02	30	100	10
NN-A6	5	1	2	0.02	30	100	10
NN-A7	5	2	2	0.02	30	100	10
NN-A8	5	3	2	0.02	30	100	10
NN-A9	5	4	2	0.02	30	100	10
NN-A10	5	5	2	0.02	30	100	10
NN-A11	5	2	1	0.02	30	100	10
NN-A12	5	2	2	0.02	30	100	10
NN-A13	5	2	3	0.02	30	100	10
NN-A14	5	2	4	0.02	30	100	10
NN-A15	5	2	5	0.02	30	100	10

Figure 2. UV spectra relating to AgNPs' formation at diverse volume ratios of (**A**) 10 mM AgNO₃ (1 to 5 mL), (**B**) 0.1 M glucose, (**C**) 0.2% starch, and (**D**) at 5 mL of different concentration of AgNO₃, (**E**) at 2 mL of various concentrations of starch, (**F**) at 2 mL of various concentrations of glucose.

The concentration of AgNO₃ (NN-A16 to NNA-20) varied from 2 to 10 mM, while the concentration of glucose (NNA-21 to NNA-25), starch (NN-A26 to NN-A30), and KOH

(NNA-31 to NNA-35) varied from 0.1 to 0.5 M, as shown in Table 2. UV spectra show the maximum absorption at 430 nm, which gradually increases with an increase in concern of $AgNO_3$ (as shown in Figure 2D–F). It is expected that a large number of Ag^+ would be available during the redox reaction, resulting in a higher yield of AgNPs, which is responsible for the increase in the absorption peak [39]. A similar behavior was observed in the UV spectra of starch, glucose, and KOH, where absorption at 430 nm gradually increases with an increase in concentrations. This result is due to an increase in the rate of nanoparticle synthesis in a highly basic environment and adequate availability of the reducing and stabilizing agent. However, in concentrated solutions the concentration of OH increases, causing aggregation on the surface AgNPs which increases in peak intensity [29,40].

Table 2. Experimental details for different concentrations. of $AgNO_3$, glucose, starch, and KOH in the synthesis of AgNPs.

Sample No	$AgNO_3$ Conc. (mM)	Starch Conc. (%)	Glucose Conc. (M)	KOH Conc. (M)	Time (min)	Temp (°C)	Stirring (rpm)
NN-A16	10	0.2	0.1	0.1	10	30	100
NN-A17	2	0.2	0.1	0.1	10	30	100
NN-A18	4	0.2	0.1	0.1	10	30	100
NN-A19	6	0.2	0.1	0.1	10	30	100
NN-A20	8	0.2	0.1	0.1	10	30	100
NN-A21	10	0.2	0.1	0.1	10	30	100
NN-A22	10	0.2	0.2	0.1	10	30	100
NN-A23	10	0.2	0.3	0.1	10	30	100
NN-A24	10	0.2	0.4	0.1	10	30	100
NN-A25	10	0.2	0.5	0.1	10	30	100
NN-A26	10	0.1	0.1	0.1	10	30	100
NN-A27	10	0.2	0.1	0.1	10	30	100
NN-A28	10	0.3	0.1	0.1	10	30	100
NN-A29	10	0.4	0.1	0.1	10	30	100
NN-A30	10	0.5	0.1	0.1	10	30	100
NN-A31	10	0.2	0.1	0.1	10	30	100
NN-A32	10	0.2	0.1	0.2	10	30	100
NN-A33	10	0.2	0.1	0.3	10	30	100
NN-A34	10	0.2	0.1	0.4	10	30	100
NN-A35	10	0.2	0.1	0.5	10	30	100

A controlled experiment without glucose and starch was carried out. UV spectrum shows that in the absence of glucose and starch absorption, 430 nm is the minimum (as shown in Figure 3B,C). This might be due to a slight reduction of Ag^+ to Ag^0 in the absence of glucose that acts as a reducing agent, whereas starch act as a stabilizing agent. In the absence of starch AgNPs are unstable and get aggregated, which results in a decrease in surface plasmon resonance peak [34]. AgNPs can form even in the absence of KOH and UV spectra reveals that absorption of AgNPs gradually increases (as given in Figure 3D), with a raise in heating time in the absence of KOH.

It can be concluded that in the absence of base pH the reaction mixture was low, hence the rate of reduction of $AgNO_3$ to AgNPs was time-consuming [41].

3.7. Possible Mechanism of the Formation of AgNPs

This reaction is an example of hydrolysis of starch that is catalyzed by a base (KOH) giving simpler molecules, like glucose. Glucose is used as a reducing agent for silver nitrate to silver metal. During the reaction, the aldehyde group of glucose reduces Ag^+ to Ag^0 and is oxidized to gluconic acid (as shown in Scheme 2), while the starch stabilizes silver nanoparticles.
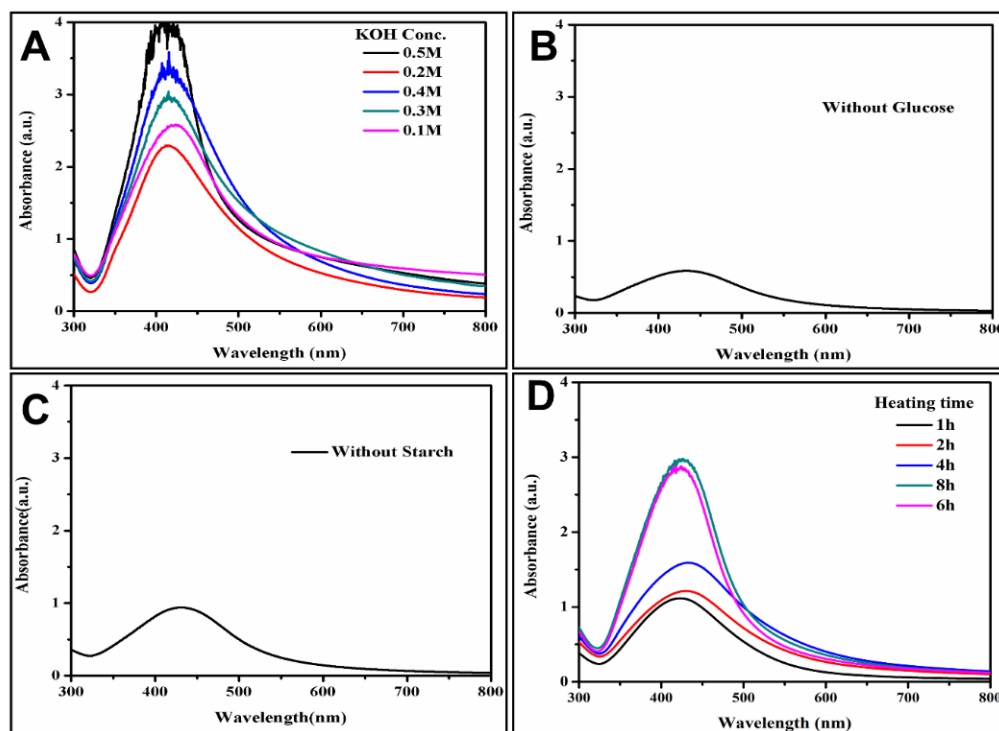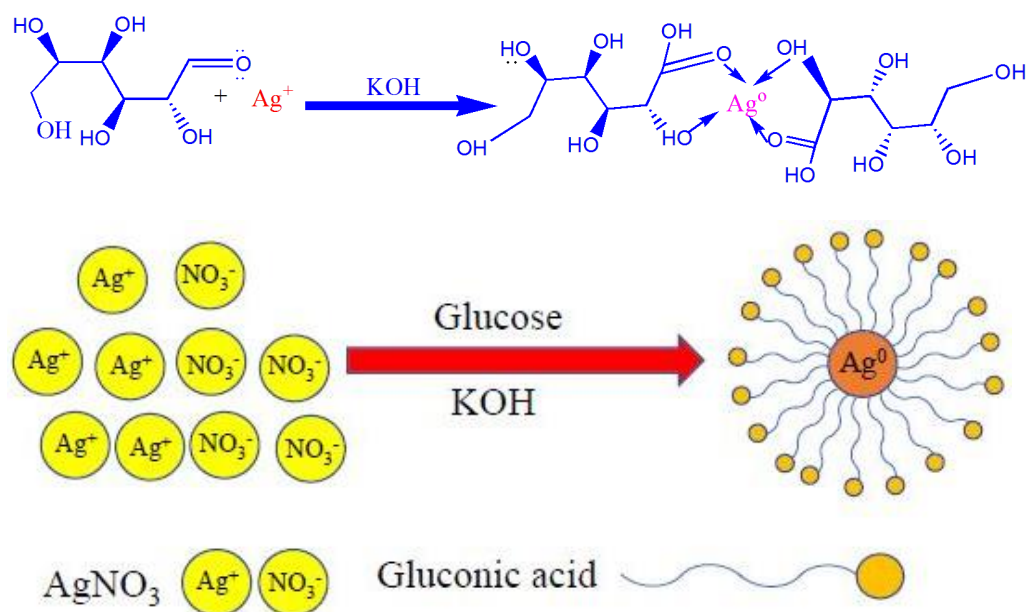
Figure 3. UV spectrum shows AgNPs formation, (**A**) at 0.02 mL of different concentrations of KOH, (**B**) without 2 mL of glucose, (**C**) without 2 mL of starch, (**D**) without 0.02 mL of KOH.


Scheme 2. Possible route for the synthesis of AgNPs.

3.8. Calorimetric Determination of Hg^{2+}

AgNPs have shown their potential in visual as well as SPR detection-based sensing of heavy metals. Herein, AgNPs are used for Hg^{2+} sensing in water. The decolorization of AgNPs and decrease in their UV absorption peak intensity is due to the redox reaction that causes the aggregation of the nanoparticles. During the reaction, Ag^0 from AgNPs is oxidized to Ag$^+$ while Hg^{2+} is reduced to Hg^0, as confirmed by the standard electrode potential values of Hg^{2+}/Hg (E$_0$ = 0.85 V) and Ag$^+$/Ag (E$_0$ = 0.79 V). Furthermore, because Hg^{2+} has a greater reduction potential than Ag+, the redox reaction 2Ag$^+$ 2Hg^{2+} = 2Ag$^+$ + Hg^{2+}

occurs spontaneously. As illustrated for the original colorless solution AgNO$_3$, oxidizing Ag^0 to Ag$^+$ changes the color of AgNPs from yellowish brown to colorless (Scheme 3). The colorimetric detection of mercury by AgNPs is based on this redox process. Ag (0) AgNPs to Ag$^+$ cannot oxidize the bulk of transition metals, alkaline, and alkaline earth metals due to their lower potential than Ag$^+$, allowing for extremely selective Hg^{2+} analyses. Thus, the oxidation of AgNPs leads to the loss of its characteristic color and a decrease in its UV absorption peak intensity.
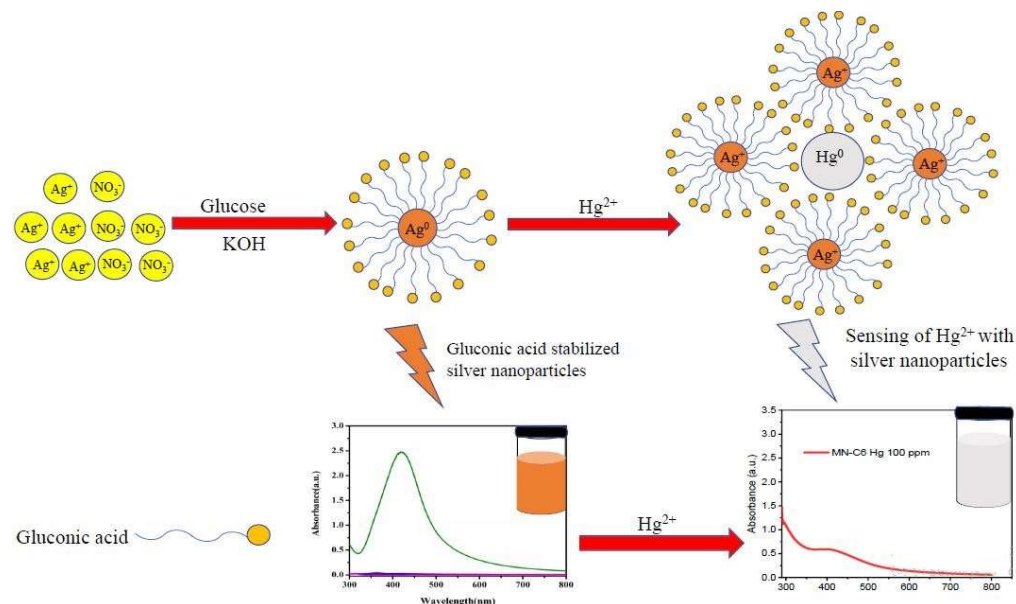
Scheme 3. The proposed mechanism of the interaction between Starch coated AgNPs and Hg^{2+} solution.

This revised mechanism promotes the mechanisms previously proposed [42–45]. However, after the addition of Hg ions, some colorimetric mercury detection methods with various surfactant or functional AgNPs might yield a colored mixture that would suggest a distinct reaction mechanism. It is found that the role of surfactant is very important during the sensing process [46]. Instead of a direct reaction between Hg^{2+} ions and Ag(0) of AgNPs, the interaction between Hg ions and capping agents (gluconic acid) to form larger nanoparticles that lead to aggregation plays a crucial role in these reactions. The interaction of Hg^{2+} ions and Ag(0) of AgNPs in the presence of gluconic acid as a surfactant is shown in Scheme 3.

3.8.1. Screening of Heavy Metals

Nanoparticles' (NP$_S$) behavior towards heavy metals was monitored by UV-Vis spectroscopy. To estimate the detection tendency of AgNPs towards heavy metals, 1 mL of AgNPs was mixed with 1 mL of aqueous solutions of heavy metals (100 ppm) under the experimental conditions reported in Table 3.

The addition of Hg^{2+} resulted in the destruction of AgNPs that was observable, as after the addition of Hg^{2+} in AgNPs, the solution suddenly changes its color from reddish yellow to colorless, as shown in vials Figure 4A. UV-Vis spectra reveals broadness and hypochromic shift in the plasmon resonance band. AgNPs dispersion shows utmost absorption intensity at 430 nm, which is dismissed by the addition of Hg^{2+} as shown in Figure 4A. All other metals, including Cu^{2+}, Na^{+1}, Cr^{+3}, Al^{3+}, Zn^{2+}, Fe^{2+}, Pb^{+2}, and Ni^{2+}, did not make any change in the color of AgNPs as well as in the UV spectrum. Hg^{2+} was the only metal that showed clear changes in color and absorption intensity of AgNPs, which may be due to the redox reaction occurring between Ag^0 and Hg^{2+}. These results reveal outstanding selectivity over a variety of heavy metals, thus AgNPs have binding sites for Hg^{2+} [42].

Table 3. Experimental details for the screening of different heavy metals by AgNPs.

Sample No	Amount of Ag NPs (mg)	Heavy Metals	Pollutants Conc (ppm)	Sensing Time (min)	Temperature (°C)	pH	Absorption Maxima (a.u.)
01	2	-	100	10	30	5	2.032
02	2	Fe^{2+}	100	10	30	5	1.778
03	2	Na^{1+}	100	10	30	5	1.682
04	2	Cr^{3+}	100	10	30	5	1.732
05	2	Cu^{2+}	100	10	30	5	1.917
06	2	Ni^{2+}	100	10	30	5	1.994
07	2	Zn^{2+}	100	10	30	5	1.789
08	2	Pb^{2+}	100	10	30	5	1.881
09	2	Al^{3+}	100	10	30	5	1.827
10	2	Hg^{2+}	100	10	30	5	0.588
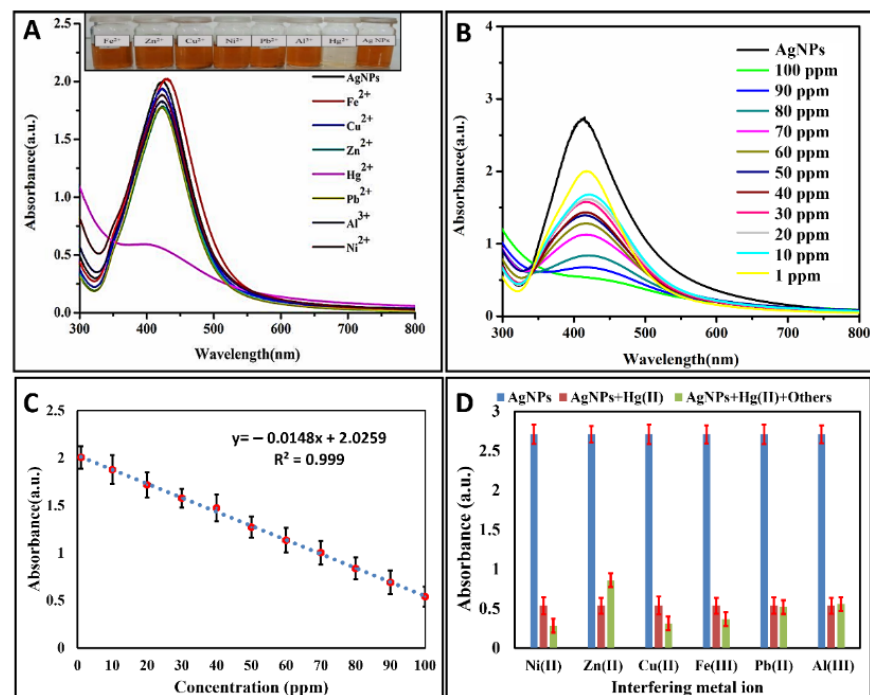
Figure 4. (**A**) Photographs and UV absorption spectra of AgNPs dispersions containing 100 ppm of Hg^{2+}, Zn^{2+}, Fe^{2+}, Pb^{2+}, Ni^{2+}, Al^{3+}, Ni^{2+}, or Cu^{2+} demonstrating the change in the color of nanoparticles upon addition of Hg^{2+}; (**B**) UV absorption spectra of AgNPs dispersions upon adding various concentrations of Hg^{2+}; (**C**) linear or direct relationship between the absorbance and Hg^{2+} concentrations; (**D**) selectivity of Ag-NPs at 430 nm: the blue bar shows the absorption intensity of AgNPs, the brown bar represents the absorption intensity of AgNPs + Hg^{2+} and the green bar represents the absorption intensity of AgNPs + Hg^{2+} in the presence of other metal ions.

3.8.2. Effect of Hg^{2+} Concentration

The quantitative estimation of the detection limit of Hg^{2+} ions sensing was studied by altering the concentrations of these Hg^{2+} (1−100 ppm) while keeping the same concentration of AgNPs at the same laboratory circumstances, as shown in Table 4.

Table 4. Experimental details for sensing of different concentrations of Hg^{2+} by Ag NPs.

Sample No	Amount of Ag NPs (mg)	Hg^{2+} Conc (ppm)	Sensing time (min)	Temperature (°C)	pH	Absorption Maxima (a.u.)
01	2	-	10	30	5	2.722
02	2	1	10	30	5	1.981
03	2	10	10	30	5	1.661
04	2	20	10	30	5	1.610
05	2	30	10	30	5	1.587
06	2	40	10	30	5	1.431
07	2	50	10	30	5	1.406
08	2	60	10	30	5	1.278
09	2	70	10	30	5	1.137
10	2	80	10	30	5	0.831
11	2	90	10	30	5	0.665
12	2	100	10	30	5	0.511

The surface plasmon resonance band of the AgNPs revealed that mixing of Hg^{2+} ions in AgNPs solutions produces a steady hypochromic shift in the surface plasmon resonance band at 430 nm. The extent of the shift in the direction of the lower-intensity depends upon the concentrations of Hg^{2+} ions, as shown in Figure 4B. The decrease in absorbance intensity was observed by an increase in the concentration of Hg^{2+} ions (1–100 ppm). It can be seen from figure that even 1 ppm concentration of Hg^{2+} produces significant reduction in the absorption intensity of AgNPS. The value of the linear regression coefficient (R2) for the system under observation was 0.998, with the theoretical detection limit up to 0.2 ppm as shown in Figure 4C. Table S1 shows the comparison of our proposed method with some recent works published in the literature (Supporting Information). These phenomena corroborate with previous results [47].

3.8.3. Interference Study with Other Metal Ions/Selectivity of the Test

To check the selectivity of the above method, 100 ppm aqueous solutions of Na^{+1}, Pb^{2+}, Cu^{2+}, Al^{3+}, Cr^{+3} Zn^{2+}, Fe^{2+}, Ni^{2+}, and Hg^{2+} were prepared. Keeping the total volume of mixture constant (3 mL), an equal volume of AgNPs, Hg^{2+} (100 ppm), and interfering metals solutions were mixed and kept at room temperature to monitor the effect. After a few minutes, the solutions of AgNPs and Hg^{2+} became colorless even in the presence of all metal ions. The hypochromic shift was observed by UV spectrum as shown in Figure 4D, which indicates that AgNPs can detect Hg^{2+} ions with high sensitivity even in the presence of an equimolar amount of other interfering cations of any other metal [48].

3.8.4. Effect of pH on Detection of Hg^{2+}

If the circumstances of the detection scheme are altered, then there is a noticeable effect on Hg^{2+} sensing. The variation in pH of the system results in aggregation and destabilization of AgNPs. The pH of the system was altered from 2 to10 by using 0.1 M KOH, and 0.1 M HCl and UV spectra were recorded for the adjusted pH values. The results indicated that AgNPs are stable in basic medium while in acidic medium (pH less than 5) the solution become colorless, and at the same time UV spectra indicate the minimum absorption intensity, as shown in Figure 5A. The stability of AgNPs in basic medium is due to an increase in the rate reduction of Ag^+ ions by OH ions from the base, which results in an augmented formation of AgNPs that is degraded by Hg^{2+} ions. It means that in basic

medium Hg^{2+} are not able to degrade the maximum amount of highly stable AgNPs, while they succeed in acidic conditions.
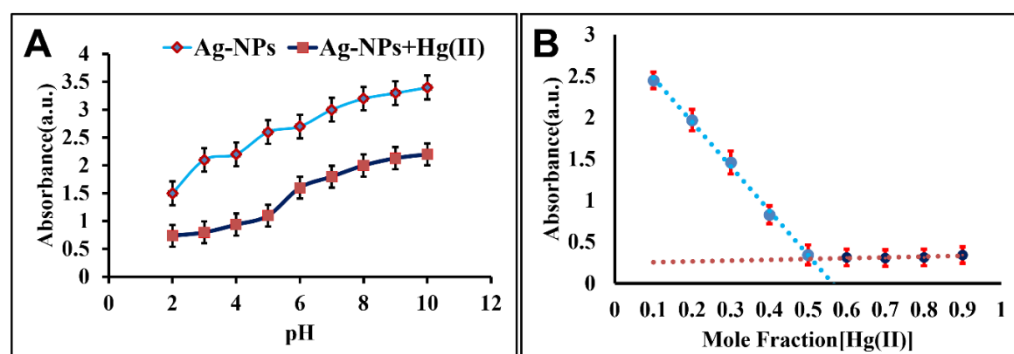

Figure 5. (**A**) Effect of pH on the adsorption of AgNPs in the absence and presence of 100 ppm Hg^{2+} ions, (**B**) Job's plot curve showing the binding ratio of AgNPs:Hg^{2+}.

3.8.5. Determination of Required Stoichiometry of AgNPs and Hg^{2+}

The binding stoichiometry of the AgNPs and Hg^{2+} was detected by Job's plot method [49]. Different mole fraction ratios of Hg^{2+} and AgNPs were tested. The absorption intensity at 430 nm obtained via UV was plotted against the molar fraction of Hg^{2+} (100 ppm) to monitor the results. The mole fraction of the highest absorption intensity revealed the binding stoichiometry of the compound. As shown in Figure 5B, 1 mL of Hg^{2+} solution and 1 mL of AgNPs suspension were present in the sample, revealing minimum absorption intensity. The results suggest that AgNPs forms a 1:1 complex (AgNPs:Hg^{2+}), which means that the best detection of heavy metals occurs when equal moles of AgNPs and Hg^{2+} are present [50]. The increased stability of AgNPs in alkaline pH might be due to stronger protection of AgNPs by deprotonated OH groups in the starch [51].

Finally, as shown in Table 2, the proposed method was applied to real tap and lake water samples. In order to verify the recovery and accuracy of the procedure, these samples were also spiked with known levels of Hg^{2+}. A volume of 1 mL of Hg^{2+} solution was added into 1 mL of tap water sample of AgNPs and after some time the solution became colorless, as was done for Hg^{2+} sensing in distilled water. Moreover, UV-visible spectra revealed that the peak became broadened at 430 nm (as shown in Figure 6) and the same results observed in distilled water are obtained. Hence, AgNPs are found to be effective for the detection of Hg^{2+} in tap water samples [52].
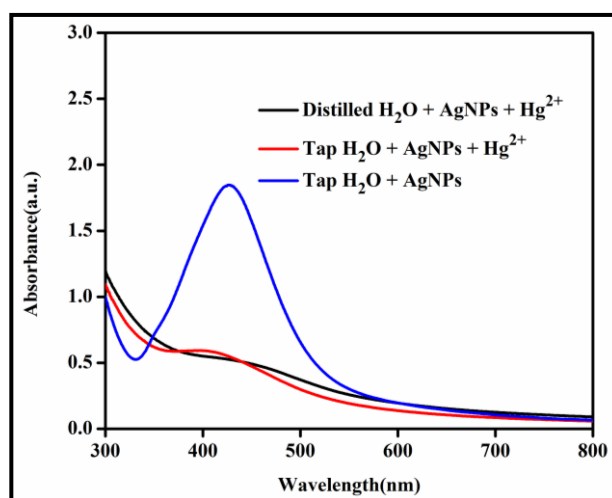

Figure 6. UV Spectrum shows detection of Hg^{2+} in laboratory tap water.

4. Conclusions

In this study, we have developed a facile and green approach for the synthesis of starch-coated silver nanoparticles-based colorimetric sensor for the selective recognition of Hg^{2+} in real samples. Various parameters that regulate the synthesis and stabilization of AgNPs were studied and optimized. The newly synthesized nanoparticles were characterized using various spectroscopic techniques. Moreover, we established the colorimetric as well as SPR detection-based sensing for Hg^{2+} by starch stabilized AgNPs. The strategy is focused on a redox reaction between Starch-AgNP and Hg^{2+}, which results in a shift in color from yellow to colorless nanoparticles dispersions and a decrease in AgNPs SPR uptake. Additionally, this approach allows a wide range of linear detection, while avoiding interference from other metal ions. The synthesized AgNPs showed admirable selectivity for Hg^{2+}, even in the occurrence of many other heavy metals. The proposed calorimetric chemosensor can be useful for laboratory tap water with a detection limit of 0.1 ppm.

References

1. Ravindran, A.; Elavarasi, M.; Prathna, T.C.; Raichur, A.M.; Chandrasekaran, N.; Mukherjee, A. Selective colorimetric detection of nanomolar Cr (VI) in aqueous solutions using unmodified silver nanoparticles. *Sens. Actuators B Chem.* **2012**, *166*, 365–371. [CrossRef]
2. Singh, R.; Thakur, P.; Thakur, A.; Kumar, H.; Chawla, P.; Rohit, J.V.; Kaushik, R.; Kumar, N. Colorimetric sensing approaches of surface-modified gold and silver nanoparticles for detection of residual pesticides: A review. *Int. J. Environ. Anal. Chem.* **2021**, *101*, 3006–3022. [CrossRef]
3. Domaille, D.W.; Que, E.L.; Chang, C.J. Synthetic fluorescent sensors for studying the cell biology of metals. *Nat. Chem. Biol.* **2008**, *4*, 168. [CrossRef] [PubMed]
4. Georgopoulos, P.G.; Roy, A.; Yonone-Lioy, M.J.; Opiekun, R.E.; Lioy, P.J. Environmental copper: Its dynamics and human exposure issues. *J. Toxicol. Environ. Health Part B Crit. Rev.* **2001**, *4*, 341–394. [CrossRef]
5. Holmes, P.; James, K.; Levy, L. Is low-level environmental mercury exposure of concern to human health? *Sci. Total Environ.* **2009**, *408*, 171–182. [CrossRef]
6. Lavoie, R.A.; Jardine, T.D.; Chumchal, M.M.; Kidd, K.A.; Campbell, L.M. Biomagnification of mercury in aquatic food webs: A worldwide meta-analysis. *Environ. Sci. Technol.* **2013**, *47*, 13385–13394. [CrossRef]
7. Manahan, S. *Fundamentals of Environmental and Toxicological Chemistry: Sustainable Science*; CRC Press: Boca Raton, FL, USA, 2013.
8. Firdaus, M.L.; Fitriani, I.; Wyantuti, S.; Hartati, Y.W.; Khaydarov, R.; McAlister, J.A.; Obata, H.; Gamo, T. Colorimetric Detection of Mercury (II) Ion in Aqueous Solution Using Silver Nanoparticles. *Anal. Sci.* **2017**, *33*, 831–837. [CrossRef]
9. Harada, M. Minamata disease: Methylmercury poisoning in Japan caused by environmental pollution. *Crit. Rev. Toxicol.* **1995**, *25*, 1–24. [CrossRef]
10. Aragay, G.; Pons, J.; Merkoçi, A. Recent trends in macro-, micro-, and nanomaterial-based tools and strategies for heavy-metal detection. *Chem. Rev.* **2011**, *111*, 3433–3458. [CrossRef]

11. Zhang, Z.; Tang, A.; Liao, S.; Chen, P.; Wu, Z.; Shen, G.; Yu, R. Oligonucleotide probes applied for sensitive enzyme-amplified electrochemical assay of mercury (II) ions. *Biosens. Bioelectron.* **2011**, *26*, 3320–3324. [CrossRef]

12. Guha, S.; Roy, S.; Banerjee, A. Fluorescent Au@ Ag core–shell nanoparticles with controlled shell thickness and HgII sensing. *Langmuir* **2011**, *27*, 13198–13205. [CrossRef] [PubMed]

13. Han, F.X.; Patterson, W.D.; Xia, Y.; Sridhar, B.B.; Su, Y. Rapid determination of mercury in plant and soil samples using inductively coupled plasma atomic emission spectroscopy, a comprehensive study. *Water Air Soil Pollut.* **2006**, *170*, 161–171. [CrossRef]

14. Fabbrizzi, L.; Licchelli, M.; Parodi, L.; Poggi, A.; Taglietti, A. The molecular design of fluorescent sensors for ionic analytes. *J. Fluoresc.* **1998**, *8*, 263–271. [CrossRef]

15. Vilder, D.S.; Jenkins, R.O.; Hall, J.F.; Harrington, C.F. The determination of methylmercury in biological samples by HPLC coupled to ICP-MS detection. *Appl. Organomet. Chem.* **2007**, *21*, 303–310.

16. Abdelhamid, H.N.; Wu, H.-F. A new binary matrix for specific detection mercury (II) using matrix-assisted laser desorption ionization mass spectrometry. *J. Am. Soc. Mass Spectrom.* **2019**, *30*, 2617–2622. [CrossRef]

17. Duan, J.; Yin, H.; Wei, R.; Wang, W. Facile colorimetric detection of Hg^{2+} based on anti-aggregation of silver nanoparticles. *Biosens. Bioelectron.* **2014**, *57*, 139–142. [CrossRef]

18. Lou, T.; Chen, L.; Zhang, C.; Kang, Q.; You, H.; Shen, D.; Chen, L. A simple and sensitive colorimetric method for detection of mercury ions based on anti-aggregation of gold nanoparticles. *Anal. Methods* **2012**, *4*, 488–491. [CrossRef]

19. Huang, J.T.; Yang, X.X.; Zeng, Q.L.; Wang, J. A simple green route to prepare stable silver nanoparticles with pear juice and a new selective colorimetric method for detection of cysteine. *Analyst* **2013**, *138*, 5296–5302. [CrossRef]

20. Yoosaf, K.; Ipe, B.I.; Suresh, C.H.; Thomas, K.G. In situ synthesis of metal nanoparticles and selective naked-eye detection of lead ions from aqueous media. *J. Phys. Chem. C* **2007**, *111*, 12839–12847. [CrossRef]

21. Li, H.; Li, F.; Han, C.; Cui, Z.; Xie, G.; Zhang, A. Highly sensitive and selective tryptophan colorimetric sensor based on 4, 4-bipyridine-functionalized silver nanoparticles. *Sens. Actuators B Chem.* **2010**, *145*, 194–199. [CrossRef]

22. Karthiga, D.; Anthony, S.P. Selective colorimetric sensing of toxic metal cations by green synthesized silver nanoparticles over a wide pH range. *RSC Adv.* **2013**, *3*, 16765–16774. [CrossRef]

23. Walekar, L.S.; Gore, A.H.; Anbhule, P.V.; Sudarsan, V.; Patil, S.R.; Kolekar, G.B. A novel colorimetric probe for highly selective recognition of Hg^{2+} ions in aqueous media based on inducing the aggregation of CPB-capped AgNPs: Accelerating direct detection for environmental analysis. *Anal. Methods* **2013**, *5*, 5501–5507. [CrossRef]

24. Wang, J.; Fang, X.; Cui, X.; Zhang, Y.; Zhao, H.; Li, X.; He, Y. A highly sensitive colorimetric probe for Cd^{2+}, Hg^{2+} and ascorbic acid determination based on trithiocyanuric acid-AuNPs. *Talanta* **2018**, *188*, 266–272. [CrossRef] [PubMed]

25. Senapati, T.; Senapati, D.; Singh, A.K.; Fan, Z.; Kanchanapally, R.; Ray, P.C. Highly selective SERS probe for Hg (II) detection using tryptophan-protected popcorn shaped gold nanoparticles. *Chem. Commun.* **2011**, *47*, 10326–10328. [CrossRef] [PubMed]

26. Chai, F.; Wang, C.; Wang, T.; Li, L.; Su, Z. Colorimetric detection of Pb^{2+} using glutathione functionalized gold nanoparticles. *ACS Appl. Mater. Interfaces* **2010**, *2*, 1466–1470. [CrossRef]

27. Ma, Y.; Jiang, L.; Mei, Y.; Song, R.; Tian, D.; Huang, H. Colorimetric sensing strategy for mercury (II) and melamine utilizing cysteamine-modified gold nanoparticles. *Analyst* **2013**, *138*, 5338–5343. [CrossRef]

28. Darbha, G.K.; Singh, A.K.; Rai, U.S.; Yu, E.; Yu, H.; Ray, P.C. Selective detection of mercury (II) ion using nonlinear optical properties of gold nanoparticles. *J. Am. Chem. Soc.* **2008**, *130*, 8038–8043. [CrossRef]

29. Miao, L.-J.; Xin, J.-W.; Shen, Z.-Y.; Zhang, Y.-J.; Wang, H.-Y.; Wu, A.-G. Exploring a new rapid colorimetric detection method of Cu^{2+} with high sensitivity and selectivity. *Sens. Actuators B Chem.* **2013**, *176*, 906–912. [CrossRef]

30. Su, W.; Yuan, S.; Wang, E. A Rhodamine-Based Fluorescent Chemosensor for the Detection of Pb^{2+}, Hg^{2+} and Cd^{2+}. *J. Fluoresc.* **2017**, *27*, 1871–1875. [CrossRef]

31. Bumagina, N.A.; Antina, E.V.; Sozonov, D.I. Off-on fluorescent sensor based on the bis (2, 4, 7, 8, 9-pentamethyldipyrrolylmethene-3-yl) methane for detection of Cd^{2+} and Hg^{2+} cations. *J. Lumin.* **2017**, *183*, 315–321. [CrossRef]

32. Ding, N.; Zhao, H.; Peng, W.; He, Y.; Zhou, Y.; Yuan, L.; Zhang, Y. A simple colorimetric sensor based on anti-aggregation of gold nanoparticles for Hg^{2+} detection. *Colloids Surf. A Physicochem. Eng. Asp.* **2012**, *395*, 161–167. [CrossRef]

33. Pienpinijtham, P.; Han, X.X.; Suzuki, T.; Thammacharoen, C.; Ekgasit, S.; Ozaki, Y. Micrometer-sized gold nanoplates: Starch-mediated photochemical reduction synthesis and possibility of application to tip-enhanced Raman scattering (TERS). *Phys. Chem. Chem. Phys.* **2012**, *14*, 9636–9641. [CrossRef] [PubMed]

34. Borbach, M.; Stenzel, W.; Conrad, H.; Bradshaw, A. Hydroxyl formation on Ag (110) studied by HREELS. *Surf. Sci.* **1997**, *377*, 796–801. [CrossRef]

35. Tagad, C.K.; Rajdeo, K.S.; Kulkarni, A.; More, P.; Aiyer, R.; Sabharwal, S. Green synthesis of polysaccharide stabilized gold nanoparticles: Chemo catalytic and room temperature operable vapor sensing application. *RSC Adv.* **2014**, *4*, 24014–24019. [CrossRef]

36. Peng, H.; Yang, A.; Xiong, J. Green microwave-assisted synthesis of silver nanoparticles using bamboo hemicelluloses and glucose in an aqueous medium. *Carbohydr. Polym.* **2013**, *91*, 348–355. [CrossRef]

37. Jyoti, K.; Baunthiyal, M.; Singh, A. Characterization of silver nanoparticles synthesized using *Urtica dioica* Linn. leaves and their synergistic effects with antibiotics. *J. Radiat. Res. Appl. Sci.* **2016**, *9*, 217–227. [CrossRef]

38. Srirangam, G.; Rao, K.P. Synthesis and charcterization of silver nanoparticles from the leaf extract of *Malachracapitata* (L). *J. Chem.* **2017**, *10*, 46–53.

39. Ismail, M.; Khan, M.; Akhtar, K.; Khan, M.A.; Asiri, A.M.; Khan, S.B. Biosynthesis of silver nanoparticles: A colorimetric optical sensor for detection of hexavalent chromium and ammonia in aqueous solution. *Phys. E Low-Dimens. Syst. Nanostruct.* **2018**, *103*, 367–376. [CrossRef]

40. Tagad, C.K.; Dugasani, S.R.; Aiyer, R.; Park, S.; Kulkarni, A.; Sabharwal, S. Green synthesis of silver nanoparticles and their application for the development of optical fiber based hydrogen peroxide sensor. *Sens. Actuators B Chem.* **2013**, *183*, 144–149. [CrossRef]

41. Meshram, S.M.; Bonde, S.R.; Gupta, I.R.; Gade, A.K.; Rai, M.K. Green synthesis of silver nanoparticles using white sugar. *IET Nanobiotechnol.* **2013**, *7*, 28–32. [CrossRef]

42. Bothra, S.; Solanki, J.N.; Sahoo, S.K. Functionalized silver nanoparticles as chemosensor for pH, Hg^{2+} and Fe^{3+} in aqueous medium. *Sens. Actuators B Chem.* **2013**, *188*, 937–943. [CrossRef]

43. Annadhasan, M.; Rajendiran, N. Highly selective and sensitive colorimetric detection of Hg (II) ions using green synthesized silver nanoparticles. *RSC Adv.* **2015**, *5*, 94513–94518. [CrossRef]

44. Wang, Y.; Yang, F.; Yang, X. Colorimetric detection of mercury (II) ion using unmodified silver nanoparticles and mercury-specific oligonucleotides. *ACS Appl. Mater. Interfaces* **2010**, *2*, 339–342. [CrossRef] [PubMed]

45. Nidya, M.; Umadevi, M.; Rajkumar, B.J. Structural, morphological and optical studies of L-cysteine modified silver nanoparticles and its application as a probe for the selective colorimetric detection of Hg^{2+}. *Spectrochim. Acta Part A Mol. Biomol. Spectrosc.* **2014**, *133*, 265–271. [CrossRef] [PubMed]

46. Chansuvarn, W.; Imyim, A. Visual and colorimetric detection of mercury (II) ion using gold nanoparticles stabilized with a dithia-diaza ligand. *Microchim. Acta* **2012**, *176*, 57–64. [CrossRef]

47. Li, L.; Feng, D.; Fang, X.; Han, X.; Zhang, Y. Visual sensing of Hg^{2+} using unmodified Au@ Ag core–shell nanoparticles. *J. Nanostruct. Chem.* **2014**, *4*, 117. [CrossRef]

48. Khan, U.; Niaz, A.; Shah, A.; Zaman, M.I.; Zia, M.A.; Iftikhar, F.J.; Nisar, J.; Ahmed, M.N.; Akhter, M.S.; Shah, A.H. Thiamine-functionalized silver nanoparticles for the highly selective and sensitive colorimetric detection of Hg^{2+} ions. *New J. Chem.* **2018**, *42*, 528–534. [CrossRef]

49. Shah, K.; ul Ain, N.; Ahmed, F.; Anis, I.; Shah, M.R. A new highly selective chemosensor for the detection of iron ion in aqueous medium based on click generated triazole. *Sens. Actuators B Chem.* **2017**, *249*, 515–522. [CrossRef]

50. Kim, H.N.; Ren, W.X.; Kim, J.S.; Yoon, J. Fluorescent and colorimetric sensors for detection of lead, cadmium, and mercury ions. *Chem. Soc. Rev.* **2012**, *41*, 3210–3244. [CrossRef]

51. Kumar, V.V.; Anbarasan, S.; Christena, L.R.; SaiSubramanian, N.; Anthony, S.P. Bio-functionalized silver nanoparticles for selective colorimetric sensing of toxic metal ions and antimicrobial studies. *Spectrochim. Acta Part A Mol. Biomol. Spectrosc.* **2014**, *129*, 35–42. [CrossRef]

52. Luo, Y.; Shen, S.; Luo, J.; Wang, X.; Sun, R. Green synthesis of silver nanoparticles in xylan solution via Tollens reaction and their detection for Hg^{2+}. *Nanoscale* **2015**, *7*, 690–700. [CrossRef] [PubMed]

53. Wang, X.; Su, Y.; Yang, H.; Dong, Z.; Ma, J. Highly sensitive fluorescence probe based on chitosan nanoparticle for selective detection of Hg^{2+} in water. *Colloids Surf. A Physicochem. Eng. Asp.* **2012**, *402*, 88–93. [CrossRef]

54. Davadhasan, J.P.; Kim, J. A chemically functionalized paper-based microfluidic platform for multiplex heavy metal detection. *Sens. Actuator B Chem.* **2018**, *10*, 18–24. [CrossRef]

55. Chen, M.-M.; Chen, L.; Li, H.-X.; Brammer, L.; Lang, J.-P. Highly selective detection of Hg^{2+} and MeHgI by di-pyridin-2-yl-[4-(2-pyridin-4-yl-vinyl)-phenyl]-amine and its zinc coordination polymer. *Inorg. Chem. Front.* **2016**, *3*, 1297–1305. [CrossRef]